1     **archiDART: an R package for the automated computation of plant root architectural traits**

2

3     Benjamin M. Delory [a], Caroline Baudson [a], Yves Brostaux [b], Guillaume Lobet [c], Patrick du Jardin [a], Loïc Pagès

4     [d], Pierre Delaplace [a, *]

5

6     [a] University of Liège – Gembloux Agro-Bio Tech. Plant Biology, Passage des Déportés, 2, B-5030 Gembloux,

7     Belgium

8     [b] University of Liège – Gembloux Agro-Bio Tech. Applied Statistics, Computer Science and Modeling, Passage

9     des Déportés, 2, B-5030 Gembloux, Belgium

10     [c] University of Liège, Laboratory of Plant Physiology, PhytoSYSTEMS, Boulevard du Rectorat, 27, B-4000,

11     Liège, Belgium

12     [d] INRA, Centre PACA, UR 1115 PSH, Domaine Saint-Paul, Site Agroparc, 84914 Avignon cedex 9, France

13

14     [*]Corresponding author: Pierre Delaplace

15     Address: University of Liège – Gembloux Agro-Bio Tech. Plant Biology, Passage des Déportés, 2, B-5030

16     Gembloux, Belgium

17     Email: Pierre.Delaplace@ulg.ac.be

18     Phone: +32-81-62.24.50

19

26      **Keywords**

27      Plant root system architecture; Data Analysis of Root Tracings (DART); Root System Markup Language (RSML);

28      2D dynamic analysis; root trait.

29

30      **Abstract**

31      *Background and Aims*

32      In order to analyse root system architectures (RSAs) from captured images, a variety of manual (e.g. Data Analysis

33      of Root Tracings, DART), semi-automated and fully automated software packages have been developed. These

34      tools offer complementary approaches to study RSAs and the use of the Root System Markup Language (RSML)

35      to store RSA data makes the comparison of measurements obtained with different (semi-) automated root imaging

36      platforms easier. The throughput of the data analysis process using exported RSA data, however, should benefit

37      greatly from batch analysis in a generic data analysis environment (R software).

38      *Methods*

39      We developed an R package (archiDART) with five functions. It computes global RSA traits, root growth rates,

40      root growth directions and trajectories, and lateral root distribution from DART-generated and/or RSML files. It

41      also has specific plotting functions designed to visualise the dynamics of root system growth.

42      *Results*

43      The results demonstrated the ability of the package's functions to compute relevant traits for three contrasted RSAs

44      (*Brachypodium distachyon* [L.] P. Beauv., *Hevea brasiliensis* Müll. Arg. and *Solanum lycopersicum* L.).

45      *Conclusions*

46      This work extends the DART software package and other image analysis tools supporting the RSML format,

47      enabling users to easily calculate a number of RSA traits in a generic data analysis environment.

48 **Introduction**

49 As water and nutrients are resources characterised by a heterogeneous spatial and temporal distribution in the soil,

50 the selection of plants able to develop a root system architecture (RSA) that optimizes water and nutrient uptake

51 in various growing conditions has been shown to be an important target for crop improvement in terms of

52 sustainable agriculture (Lynch 1995; de Dorlodot et al. 2007; Den Herder et al. 2010; Meister et al. 2014). In this

53 context, linking genotypes and environmental conditions to phenotypes requires the use of high-throughput plant

54 phenotyping platforms that allow a quantitative analysis of a large number of plants on which an increasing number

55 of traits can be accurately measured (Cobb et al. 2013; Fiorani and Schurr 2013). Due to its complexity and

56 belowground localisation, however, phenotyping a root system is challenging and numerous tools are being

57 developed to address this difficulty. These tools are part of a processing chain that consists of three main steps: (1)

58 high-resolution imaging of excavated (2D) or undisturbed (2D or 3D) root systems, (2) recognition of the relevant

59 biological structures in the captured images (Zhu et al. 2011), and (3) calculation of static and dynamic features

60 that describe the RSA either locally (for an individual root, a specific root class, etc.) or globally (at the whole root

61 system scale) (de Dorlodot et al. 2007; Clark et al. 2011; Nagel et al. 2012). Using high-resolution images acquired

62 with light or confocal microscopes (Wells et al. 2012; Slovak et al. 2014), flatbed scanners (Pagès 2014), digital

63 cameras (Le Marié et al. 2014; Mathieu et al. 2015) or non-invasive 3D techniques such as X-ray computed

64 tomography and magnetic resonance imaging (Zhu et al. 2011), software packages can be used for the detection

65 of roots on captured images prior to the calculation of relevant RSA traits. Depending on the level of interaction

66 between the user and the imaging software, root detection can be performed manually (Le Bot et al. 2010), semi-

67 automatically (Lobet et al. 2011; Clark et al. 2013; Pound et al. 2013) or fully automatically (French et al. 2009;

68 Iyer-Pascuzzi et al. 2010; Wells et al. 2012; Diener et al. 2013; Kumar et al. 2014; Leitner et al. 2014; Pace et al.

69 2014; Slovak et al. 2014; Bucksch et al. 2014; Cai et al. 2015). The use of a manual tracing software tool like Data

70 Analysis of Root Tracings (DART) is well suited for the 2D analysis of mature root systems with a high level of

71 root overlaps or for rhizotron images, but it is not suitable in a high-throughput phenotyping context for which

72 scientists will prefer automated or semi-automated tracing tools. As a consequence of the variety of 2D image

73 analysis software solutions dedicated to the analysis of RSAs [listed in the Plant Image Analysis Database, (Lobet

74 et al. 2013)], the comparison of measurements acquired with different platforms is often difficult, mainly because

75 these platforms do not compute the same RSA traits and the stored RSA data do not share a common structure. In

76 order to partly solve this problem, the Root System Markup Language (RSML) has been recently introduced as a

77 convenient way to store and exchange RSA data in a standardized format (Lobet et al. 2015). At the time of writing,

78    a RSML support has been implemented in two semi-automated (SmartRoot and RootNav) and three automated

79    (RootTrace, RhizoScan and RootSystemAnalyser) 2D root image analysis software tools. As manual, semi-

80    automated and fully automated root tracing solutions offer complementary approaches to study RSAs and generate

81    large datasets from which relevant RSA traits can be calculated, it would be of great interest to develop a tool

82    allowing the batch analysis of DART-generated and/or RSML files using automated procedures in a generic data

83    analysis environment that allows easy access to the calculated RSA traits for further statistical analyses (Table 1).

84    In order to achieve this goal, we developed an R package (**archiDART**) for the computation of global RSA traits

85    (root length, root number, etc.) at each observation date, root growth directions and trajectories (branching and

86    root tip angles, root curvature), and lateral root length and density distribution from DART and RSML files (Delory

87    et al. 2015). The package also enables the dynamics of root system growth and local root growth rate variations to

88    be visually assessed using specific plotting and mapping functions. In this paper, our objective was to present the

89    main functionalities of archiDART and demonstrate the added value of this package using contrasted RSAs.

90

91    **Materials and Methods**

92    In order to illustrate the functionalities of the R package archiDART, we performed a quantitative root system

93    architecture analysis of a model cereal (*Brachypodium distachyon* [L.] P. Beauv.) and two dicotyledonous plant

94    species (*Hevea brasiliensis* Müll. Arg. and *Solanum lycopersicum* L.) produced under various growing conditions

95    and we focused our analysis on selected root traits that were particularly relevant for each plant species.

96

97              Example 1: Time series images of *Brachypodium* plantlets exposed to rhizobacterial volatiles *in vitro*

98    In order to show the impact of volatile compounds emitted by plant growth-promoting rhizobacteria (PGPR)

99    commonly found in the plant's rhizosphere on the RSA of a model cereal, eight root systems of *B. distachyon*

100   plantlets were produced *in vitro* in square petri dishes on a Hoagland medium and were either co-cultivated with

101   one PGPR strain (*Bacillus pumilus* C26, *Bacillus subtilis* AP305-GB03 or *Enterobacter cloaceae* AP12-JM22) or

102   cultivated alone following the protocol described by Delaplace et al. (2015), except that the photoperiod used in

103   the growth chamber was 16 h/8 h − L/D and the lateral roots were detected without setting a minimal length

104   threshold. Monitoring the RSA of each plantlet started at the beginning of the experiment (day 0) and was

105   performed by scanning each root system at 400 dpi every 24 h for 11 days. At the end of the experiment (day 11),

106   a single composite image of each root system was constructed with Adobe Photoshop 7.0.1 (Adobe Systems

107    Incorporated, San Jose, CA, USA). In order to facilitate the vectorization with DART, the new root segments that

108    appeared at each observation date were drawn with a specific colour.

109

110            Example 2: Time series images of the root system of a rubber tree growing in a rhizotron

111    The root system of this rubber tree species was produced in a vertical root observation box filled with 2 mm-sieved

112    vermiculite. The development of the root system was monitored every 2 days by drawing the new growth

113    increments on a transparent plastic sheet using a unique colour for each observation date. The RSA used in this

114    work was that of a 37-day-old *H. brasiliensis* seedling (Thaler and Pagès 1996a).

115

116            Example 3: Time series images of a tomato root system produced hydroponically

117    As a third example, we used the root system of a tomato plant produced hydroponically in a horizontal flat box, as

118    described by Le Bot et al. (2010). Images of the entire root system were taken every 24 h using a digital camera.

119    The RSA used in this work was that of a 28-day-old tomato plant.

120

121            RSA input data

122    Two types of RSA input data can be used to compute RSA traits with the R package archiDART (Table 1): (1) the

123    files exported by Data Analysis of Root Tracings (DART) (Le Bot et al. 2010) and (2) RSA data encoded with the

124    Root System Markup Language (RSML) (Lobet et al. 2015). Although DART-generated and RSML files do not

125    share a common structure, the functions of our R package use the file extensions to discriminate between these

126    two file types and compute RSA traits for each independently, allowing the batch analysis of DART-generated

127    and RSML files in a single operation.

128    In this paper, the images showing the RSA of each plant species were processed with DART and the files

129    containing topological (file extension: .rac), temporal (file extension: .tps) and spatial (file extension: .lie)

130    attributes were saved into a specific folder for each plant species after the manual vectorization of each root system.

131    The RSAs were then analysed with the archiDART 1.1 package (Delory et al. 2015) using the 3.2.0 version of R

132    statistical software (R Core Team 2015).

133        Overview of the package's functions

134    The archiDART package (version 1.1) has five functions (*archidraw*, *archigrow*, *architect*, *latdist* and *trajectory*)

135    that allow the batch processing of many root systems by simply knowing (1) the path(s) to the folder(s) containing

136    the DART-generated and/or the RSML files exported by another root imaging software tool supporting this file

137    format, (2) the unit of length and unit of time that should be used by the functions in order to perform the

138    calculations and express the results, and (3) the resolution of the images used to vectorize the root systems (if

139    images were acquired with a flatbed scanner; resolution is expressed in dots/inch) or the ratio between the length

140    of a reference object located on the image expressed in pixels and the actual length of the same object expressed

141    in inches (if images were acquired with a digital camera) (Delory et al. 2015). An overview of the required files,

142    returned R objects and calculated RSA traits for each R function of the package is shown in Table 1. A full

143    description of the values taken by each function is in the documentation files provided with the R package

144    (http://cran.r-project.org/package=archiDART).

145    The graphical functions *archidraw* and *archigrow* allow the X-Y plotting of each vectorized root system for

146    selected observation dates. They both use the generic X-Y plotting functions of the R package 'graphics' (R Core

147    Team 2015) to plot the vectorization results of many root systems in a single operation. Whereas *archidraw* is a

148    plotting function that allows the graphical representation of a root system with a colour code depending on the

149    observation date at which a link is seen for the first time, *archigrow* allows both the exportation of growth rate

150    matrices and the X-Y plotting of vectorized root systems with a colour code depending on the growth rate value

151    of each link constituting the vectorized root systems. The *archigrow* function computes root growth rates following

152    the method described in Table 2. Using these functions, the user can easily customize the graphical outputs by

153    setting additional graphical parameters.

154    The *architect* function was designed for the one-step calculation of a number of integrated RSA traits in order to

155    provide an overall description of entire root systems at each observation date (Table 1). Root lengths, root numbers

156    and lateral root densities are computed by the *architect* function according to the methods described in Table 2. In

157    addition to these parameters, the secondary root distribution along a first-order root can also be studied with

158    *architect*. To do so, one has to delimit zones along the first-order root before running the function using the rootdiv

159    argument. The total secondary root length, the total number of secondary roots and the secondary root density will

160    then be computed for each zone on the first-order root. The calculated RSA parameters are stored in a data frame

161    that can easily be used for subsequent statistical analyses with R or other statistical software.

162     The purpose of the *latdist* function is to describe lateral root length and density distribution along each mother root

163     of a vectorized root system (Table 2). To do so, the function use the distance between each branching point to the

164     parent root base (DBase, Fig. 1a) in order to select the daughter roots to be used for calculating local lateral root

165     lengths and densities along each parent root. Using the *latdist* function comprises two main steps. First, the function

166     selects the points along the parent roots on which the calculation of RSA parameters should be performed.

167     Depending on user choice, these points can be selected with or without linear interpolation. The use of interpolated

168     points allows a more continuous evaluation of the lateral root length and density distribution on each parent root.

169     Lateral root density and a total lateral root length are then calculated at intervals of a length defined by the

170     experimenter and centred on each selected point. At the end of the calculation process, the results are stored in a

171     list, giving easy access to the computed RSA traits for each mother root of each analysed root system. A second

172     algorithm for measuring the inter-branch distances was also incorporated to *latdist* (Table 2).

173     With regard to the importance of root growth directions and trajectories in RSA, the *trajectory* function was

174     designed to calculate root growth angle (basal branching and root tip angles), orientation and tortuosity, as well as

175     statistical parameters (mean and standard deviation) that describe the curvature of each root of a vectorized root

176     system. These RSA traits are computed by the *trajectory* function following the methods described in Table 2. As

177     the orientation of the vectorized root system can be different from that of the natural plant root system depending

178     on the device used to acquire root images, one can specify an angle value that will be used by the function to rotate

179     the vectorized root system clockwise before calculating the RSA parameters. Because the angle values computed

180     by *trajectory* depend on the initial values of l.brangle and l.tipangle (Table 2), these must be carefully chosen

181     before running the function and will be notably linked to the plant species studied. The curvature of a root can be

182     evaluated by its tortuosity. In addition, *trajectory* also allows the computation of statistical parameters (mean and

183     standard deviation) that characterise the distribution of local angles measured at selected points linearly

184     interpolated along a root. The method used by *trajectory* to calculate local angles on a root is very similar to that

185     used in RootTrace (French et al. 2009) and comprises three main steps. First, the function will position

186     equidistantly spaced points along each root constituting a vectorized root system. The distance between the

187     interpolated points (l.curv) is set by the user before running the *latdist* function. Second, the angles ($\theta_{ij}$) between

188     the direction vectors ($\overrightarrow{H_{ij}}$) of successive links along each root are calculated (Fig. 1d). As pointed out by French et

189     al. (2009), a high $\theta_{ij}$ value is associated with a pronounced local curvature. The mean and standard deviation of

190     the calculated angles are then determined for each root. As the user-defined distance between the interpolated

191     points (l.curv) affects the computed local angles between successive direction vectors, the initial value of this

192    parameter should be carefully chosen by the experimenter before carrying out the function in order to best fit the

193    RSA of the considered plant.

194

195    **Results**

196        *archidraw*: X-Y plotting of vectorized root systems

197    In order to qualitatively compare several RSA across time series experiments and export the vectorized root

198    systems as high-resolution images, we developed an R function allowing the X-Y plotting of each vectorized root

199    system for selected observation dates. As an example, we used *archidraw* to plot the RSA of a 12-day-old *B.*

200    *distachyon* plantlet produced *in vitro* and exposed to the volatiles emitted by *B. subtilis* AP305-GB03 (Example

201    1, Fig. 2a), the RSA of a 37-day-old rubber tree produced in a vertical rhizotron (Example 2, Fig. 2b) and part of

202    the RSA of a 28-day-old tomato plant produced hydroponically in a horizontal flat box (Example 3, Fig. 2c). The

203    last-mentioned RSA was plotted with a specific colour for each observation date.

204

205        *archigrow*: computing growth rate matrices and X-Y plotting of vectorized root systems

206    As the graphical outputs exported by *archidraw* did not allow the visual detection of the root system parts that

207    were characterised by high or low growth rate values, we developed a second mapping function (*archigrow*)

208    allowing both the exportation of growth rate matrices and the X-Y plotting of vectorized root systems for selected

209    observation dates with a colour code depending on the growth rate value of each link constituting the vectorized

210    root systems. Such a tool could be particularly useful for rapidly screening local growth rate variations between

211    analysed root systems. As an example, we used *archigrow* to study the growth rate variations between four root

212    systems of *B. distachyon* plantlets that were or not exposed to rhizobacterial-emitted volatiles (Example 1). The

213    results showed that plants exposed to bacterial volatiles were characterised by higher growth rate values for the

214    primary root and the first-order lateral roots (Fig. 3).

215

216        *architect*: computing parameters describing the global RSA

217    In order to quantitatively compare the architecture of many root systems, it is often useful to start the data analysis

218    process by calculating the RSA traits that provide a global description of each root system. In this way, *architect*

219    is an R function performing a one-step calculation of common RSA traits for each analysed root system at each

220    observation date. To illustrate this R function, we used *architect* on the DART files associated with the *B.*

221    *distachyon* root systems (Example 1) and we plotted the results for three RSA parameters showing contrasted

222    results between experimental treatments (Fig. 4). The use of *architect* allowed a rapid analysis of the effects of

223    rhizobacterial volatiles on the RSA of *B. distachyon* plantlets. As shown in the figures, the root system of plants

224    exposed to rhizobacterial volatiles had a higher growth rate (Fig. 4a), a higher number of lateral roots (Fig. 4b)

225    and a greater length of first-order lateral roots (Fig. 4c) than the control plants at the end of the experiment. These

226    results confirm the growth rate variations observed between experimental treatments using the mapping function

227    *archigrow* (Fig. 3). Both *architect* and *archigrow* can be used to compare the growth kinetics of root systems but

228    these two functions will not have the same spatial resolution when computing root growth rates. Whereas *architect*

229    allows the computation of growth rates for the entire root system or for each branching order at each observation

230    date, the growth rate matrices and the graphical outputs exported by *archigrow* allow an analysis of the entire root

231    system growth with a far higher spatial resolution because a 'root by root' analysis can be performed.

232

233            *latdist*: computing lateral root length and density distribution

234    As DART is a software package that can provide length and topological information for each root of a vectorized

235    root system (Le Bot et al. 2010), notably via a distance calculated between each branching point and the

236    corresponding parent root base (DBase, Fig. 1a), an algorithm that could convert this information into lateral root

237    length and density distribution on each mother root would be a valuable tool for RSA analysis. In order to illustrate

238    the outputs calculated by *latdist*, we used it on four root systems of *B. distachyon* plantlets that were or were not

239    exposed to rhizobacterial volatiles (Example 1, Fig. 5), as well as on the root system of a rubber tree that had

240    shown periodicity in lateral root development (Example 2, Fig. 6) (Thaler and Pagès 1996b). For clarity reasons,

241    the results plotted in Fig. 5 and 6 show only the evolution of lateral root density, the lateral root length and the

242    distance between neighbouring lateral roots for the primary root. For *B. distachyon*, a maximum lateral root density

243    of 11-13 roots/cm was reached in a zone localized between 1.2 and 1.8 cm from the primary root base and no clear

244    difference emerged when the four root systems were compared for that variable (Fig. 5, a-d) or for the distances

245    between neighbouring lateral roots (Fig. 5, i-l). As for the total length of the first-order lateral roots, this showed

246    a maximum value localized between 1.1 and 1.6 cm, which parallels the results obtained for lateral root density

247    distribution. When the results were compared for that primary root zone, it was evident that total secondary root

248    length was lower for the control plant (2.2 cm of secondary roots/cm of primary root) than for the plants exposed

249    to rhizobacterial volatiles (5.1-5.6 cm of secondary roots/cm of primary root), confirming that the lateral root

250    elongation rate was lower for the unexposed plant (Fig. 5, e-h). In a second example, we tested the ability of *latdist*

251    to detect a periodic pattern in the lateral root development of a rubber tree, as described by Thaler and Pagès

252    (1996b). Three first-order lateral root density maxima were visually detected along the taproot of the rubber tree

253    (Fig. 6a). The first maximum (9 roots/cm) was located between 0.7 and 1 cm from the taproot base. This local

254    maximum was associated with secondary roots that started to develop early (Le Roux and Pagès 1994). Two

255    additional local maxima associated with acropetal first-order lateral roots were also detected at 6.9 (8 roots/cm)

256    and 27.7 cm (8 roots/cm) from the taproot base. The secondary root length distribution along the taproot paralleled

257    the lateral root density distribution with high and low lateral root lengths calculated in zones with high or low

258    branching densities, respectively (Fig. 6b). The use of the *archigrow* function to study the evolution of lateral root

259    vigour along the taproot showed that highly branched areas with high lateral root growth rates alternated with

260    poorly branched areas characterised by low lateral root growth rates (Fig. 7). Taken together, these results

261    demonstrate the ability of *latdist* and *archigrow* to detect a periodic developmental process in a rubber tree for

262    first-order lateral root emergence and elongation, as previously demonstrated by Thaler and Pagès (1996b).

263

264         *trajectory*: computing RSA traits describing root growth directions and trajectories

265    The *trajectory* R function was designed for calculating root traits that describe root growth directions and

266    trajectories. To illustrate some outputs of *trajectory*, we used the function on the DART files associated with the

267    root system of a 37-day-old rubber tree (Example 2). First, we compared the branching angles of the main root

268    types identified by Le Roux and Pagès (1994) (Fig. 8a). The results showed that the branching angles of early and

269    acropetal secondary roots had median values of 59.2° and 70.8°, respectively. By contrast, the tertiary roots had a

270    higher median value (82.3°) and greater variability than the branching angles measured for the secondary roots.

271    Second, we studied the potential of *trajectory* to follow the root tip angle of selected roots growing in a vertical

272    rhizotron for 34 days (Fig. 8b). For clarity reasons, in the figure the evolution of the root tip angle during the

273    cultivation period is shown only for the taproot, the two longest early secondary roots and the two longest acropetal

274    secondary roots. The results showed that the taproot grew almost vertically with a root tip angle of 4.3° ± 4.5°

275    (mean ± sd). Compared with the acropetal secondary roots, the two analysed early secondary roots seem to grow

276    with a steeper root tip angle. It can also be seen that one of the acropetal secondary roots grew with a negative

277    gravitropism at the end of the experiment because its registered root tip angle at the last observation date was

278    greater than 90° (92.7°).

**Discussion**

279

280     In this paper, we presented five functions of an R package (archiDART, version 1.1) designed for the automated

281     computation of RSA traits from data exported by manual (DART) or semi- and fully automated root image analysis

282     platforms that have been implemented with a Root System Markup Language (RSML) support. Considering the

283     increasing number of root image analysis tools, the RSML was introduced as a convenient way to store and

284     exchange RSA data between imaging software tools (Lobet et al. 2015; Lobet 2015). In order to allow the analysis

285     of RSML files with the archiDART package, an import function has been implemented in *architect*, *archidraw*,

286     *latdist* and *trajectory*. Briefly, this function converts the RSA data encoded in each RSML file into data frames

287     possessing the same structure as the files generated by DART before calculating the RSA traits. This import

288     function allows the processing of RSML files and extends the use of the archiDART package to RSA data that

289     were exported with root imaging software tools supporting this file format (Fig. 9). Therefore, as the functions of

290     the archiDART package can use the spatial and topological information stored in both DART and RSML files to

291     compute relevant RSA traits, this tool allows the comparison of root systems skeletonized with different root

292     tracing solutions and complements these software packages with the possibility to compute new RSA traits. When

293     coupled with DART or root imaging software tools supporting the RSML format, the archiDART package

294     improves the RSA analysis process by allowing the batch analysis of many root systems and the computation of

295     relevant parameters aimed at describing each analysed RSA at both a global and a local scale. To date, the

296     package's functionalities include the computation of RSA traits and graphical outputs that allow (1) a global and

297     dynamic analysis of root system growth (*architect, archidraw*), (2) an efficient description and mapping of growth

298     rate variations between components of a single or many root systems (*archigrow*), (3) a detailed analysis of lateral

299     root length and density distribution along the mother roots of each analysed root system (*latdist*), and (4) a

300     comprehensive analysis of root growth directions and trajectories via the calculation of branching and root tip

301     angles, as well as parameters characterising root curvature (*trajectory*).

302     The choice of a root tracing solution for the analysis of root system architectures is conditioned by the quality and

303     the number of root images, the level of automation required by the experimenter, as well as the RSA traits that

304     should be measured on captured images. Although most root imaging platforms deal with root number and root

305     length measurements, other RSA traits that are computed by a limited number of platforms can be more relevant

306     to analyse in certain situations. Among all the parameters that can be calculated by the archiDART package, lateral

307     root length and density distribution are two important RSA traits for at least two reasons. First, as roots compete

308     with each other for shared internal resources, the optimal number of lateral roots will be related to the balance

309  between their metabolic costs and the need for root development and resource acquisition (Lynch 2013). Second,

310  as mobile resources (e.g., water and nitrates) are more efficiently taken up by long but dispersed laterals and

311  immobile resources (e.g., phosphorus) are more efficiently acquired by fine but dense laterals, these RSA features

312  will determine the balance between mobile and immobile resource uptake (López-Bucio et al. 2003; Malamy 2005;

313  Lynch 2013). In addition, as resource acquisition by plant roots is challenged by a heterogeneous spatial and

314  temporal distribution of water and nutrients in the soil (Lynch 1995; Giehl et al. 2014), root growth direction and

315  trajectories also play an important role in the development of RSA, but only a few root imaging platforms are able

316  to compute such traits (Lobet et al. 2013). Among the possible parameters aimed at describing RSA, root growth

317  angles are of major importance in resource foraging and depend on root type, edaphic conditions and genotype

318  (Rich and Watt 2013; Wu et al. 2014). As shallow and steep root growth angles are associated with topsoil and

319  deep foraging strategies, respectively, root growth angles will condition the soil layers that will be explored by

320  plant roots (Forde and Lorenzo 2001; Lynch 2013; Uga et al. 2013). Root growth direction has also been shown

321  to be an important RSA feature in plant – plant interaction studies, which have revealed that individuals growing

322  next to each other can sense the presence of neighbours and are able to orient their root development accordingly

323  (de Kroon 2007; Gonkhamdee et al. 2010; Rascher et al. 2011; Faget et al. 2013; Schmid et al. 2015). Because of

324  its complementarity with several root tracing solutions, the use of archiDART can help scientists to choose the

325  most appropriate root image analysis software tool without uniquely focusing on the RSA traits computed by these

326  software packages.

327  In recent years, root models have become an important tool in root research (Godin and Sinoquet 2005). However,

328  the main limitation in using these models is often the lack of quantitative data. Our R package archiDART can

329  help overcome this issue by providing modellers with useful metrics. Typically, dynamic variables (e.g. growth

330  rates), often used as input parameters in root models (Pagès et al. 2013), can be generated using

331  archiDART. Moreover, density distribution, growth rate and direction can also be used in density-based models

332  (Dupuy et al. 2010).

333  The functions of the archiDART package have been shown to work efficiently for the computation and analysis

334  of RSA traits of both monocotyledonous (*B. distachyon*) and dicotyledonous plant species (*H. brasiliensis* and *S.*

335  *lycopersicum*) produced under various growing conditions. Considering that manual, semi-automated and fully

336  automated root tracing solutions offer complementary approaches for the analysis of RSAs, archiDART extends

337  the DART software package and other image analysis tools supporting the RSML format, enabling users to easily

338  calculate a number of RSA traits in a generic data analysis environment for further statistical analyses. As an R

339 package, it has a detailed documentation file for each function and is freely downloadable from the CRAN

340 repository (http://cran.r-project.org/package=archiDART).

341

342 **Conflict of Interest**: The authors declare that they have no conflict of interest.

343

344 **References**

345 Bucksch A, Burridge J, York LM, et al. (2014) Image-based high-throughput field phenotyping of crop roots. Plant
346   Physiol 166:470–486. doi: 10.1104/pp.114.243519

347 Cai J, Zeng Z, Connor JN, et al. (2015) RootGraph : a graphic optimization tool for automated image analysis of
348   plant roots. J Exp Bot. doi: 10.1093/jxb/erv359

349 Clark RT, Famoso AN, Zhao K, et al. (2013) High-throughput two-dimensional root system phenotyping platform
350   facilitates genetic analysis of root growth and development. Plant Cell Environ 36:454–466. doi:
351   10.1111/j.1365-3040.2012.02587.x

352 Clark RT, MacCurdy RB, Jung JK, et al. (2011) Three-dimensional root phenotyping with a novel imaging and
353   software platform. Plant Physiol 156:455–465. doi: 10.1104/pp.110.169102

354 Cobb JN, DeClerck G, Greenberg A, et al. (2013) Next-generation phenotyping : requirements and strategies for
355   enhancing our understanding of genotype-phenotype relationships and its relevance to crop improvement.
356   Theor Appl Genet 126:867–887. doi: 10.1007/s00122-013-2066-0

357 De Dorlodot S, Forster B, Pagès L, et al. (2007) Root system architecture: opportunities and constraints for genetic
358   improvement of crops. Trends Plant Sci 12:474–481. doi: 10.1016/j.tplants.2007.08.012

359 De Kroon H (2007) How do roots interact? Science 318:1562–1563. doi: 10.1126/science.1150726

360 Delaplace P, Delory BM, Baudson C, et al. (2015) Influence of rhizobacterial volatiles on the root system
361   architecture and the production and allocation of biomass in the model grass *Brachypodium distachyon* (L.)
362   P. Beauv. BMC Plant Biol 15:1–15. doi: 10.1186/s12870-015-0585-3

363 Delory BM, Baudson C, Brostaux Y, et al. (2015) archiDART: Plant Root System Architecture Analysis Using
364   DART and RSML Files. R package version 1.1. http://CRAN.R-project.org/package=archiDART.

365 Den Herder G, Van Isterdael G, Beeckman T, De Smet I (2010) The roots of a new green revolution. Trends Plant
366   Sci 15:600–607. doi: 10.1016/j.tplants.2010.08.009

367 Diener J, Nacry P, Périn C, et al. (2013) An automated image-processing pipeline for high-throughput analysis of
368   root architecture in OpenAlea. 7th Int. Conf. Funct. Plant Model. Sariselkä, Finland, pp 85–87

369 Dupuy L, Gregory PJ, Glyn Bengough A (2010) Root growth models: Towards a new generation of continuous
370   approaches. J Exp Bot 61:2131–2143. doi: 10.1093/jxb/erp389

371 Faget M, Nagel KA, Walter A, et al. (2013) Root-root interactions: extending our perspective to be more inclusive
372   of the range of theories in ecology and agriculture using in-vivo analyses. Ann Bot 112:253–266. doi:
373   10.1093/aob/mcs296

374 Fiorani F, Schurr U (2013) Future scenarios for plant phenotyping. Annu Rev Plant Biol 64:267–291. doi:
375   10.1146/annurev-arplant-050312-120137

376  Forde B, Lorenzo H (2001) The nutritional control of root development. Plant Soil 232:51–68. doi:
377      10.1023/A:1010329902165

378  French A, Ubeda-Tomás S, Holman TJ, et al. (2009) High-throughput quantification of root growth using a novel
379      image-analysis tool. Plant Physiol 150:1784–1795. doi: 10.1104/pp.109.140558

380  Giehl RFH, Gruber BD, von Wirén N (2014) It's time to make changes: modulation of root system architecture
381      by nutrient signals. J Exp Bot 65:769–778. doi: 10.1093/jxb/ert421

382  Godin C, Sinoquet H (2005) Functional – structural plant modelling. New Phytol 166:705–708.

383  Gonkhamdee S, Pierret A, Maeght J-L, et al. (2010) Effects of corn (*Zea mays* L.) on the local and overall root
384      development of young rubber tree (*Hevea brasiliensis* Muel. Arg). Plant Soil 334:335–351. doi:
385      10.1007/s11104-010-0386-2

386  Iyer-Pascuzzi AS, Symonova O, Mileyko Y, et al. (2010) Imaging and analysis platform for automatic phenotyping
387      and trait ranking of plant root systems. Plant Physiol 152:1148–1157. doi: 10.1104/pp.109.150748

388  Kumar P, Huang C, Cai J, Miklavcic SJ (2014) Root phenotyping by root tip detection and classification through
389      statistical learning. Plant Soil 380:193–209. doi: 10.1007/s11104-014-2071-3

390  Le Bot J, Serra V, Fabre J, et al. (2010) DART: a software to analyse root system architecture and development
391      from captured images. Plant Soil 326:261–273. doi: 10.1007/s11104-009-0005-2

392  Le Marié C, Kirchgessner N, Marschall D, et al. (2014) Rhizoslides : paper-based growth system for non-
393      destructive, high throughput phenotyping of root development by means of image analysis. Plant Methods
394      10:1–16. doi: 10.1186/1746-4811-10-13

395  Le Roux Y, Pagès L (1994) Développement et polymorphisme racinaires chez de jeunes semis d'hévéa (*Hevea
396      brasiliensis*). Can J Bot 72:924–932.

397  Leitner D, Felderer B, Vontobel P, Schnepf A (2014) Recovering root system traits using image analysis
398      exemplified by two-dimensional neutron radiography images of lupine. Plant Physiol 164:24–35. doi:
399      10.1104/pp.113.227892

400  Lobet G (2015) rsml: Plant Root System Markup Language (RSML) File Processing. R package version 1.2.
401      http://CRAN.R-project.org/package=rsml.

402  Lobet G, Draye X, Périlleux C (2013) An online database for plant image analysis software tools. Plant Methods
403      9:1–7. doi: 10.1186/1746-4811-9-38

404  Lobet G, Pagès L, Draye X (2011) A novel image-analysis toolbox enabling quantitative analysis of root system
405      architecture. Plant Physiol 157:29–39. doi: 10.1104/pp.111.179895

406  Lobet G, Pound MP, Diener J, et al. (2015) Root System Markup Language : toward an unified root architecture
407      description language. Plant Physiol 167:617–627. doi: 10.1104/pp.114.253625

408  López-Bucio J, Cruz-Ramírez A, Herrera-Estrella L (2003) The role of nutrient availability in regulating root
409      architecture. Curr Opin Plant Biol 6:280–287. doi: 10.1016/S1369-5266(03)00035-9

410  Lynch J (1995) Root architecture and plant productivity. Plant Physiol 109:7–13.

411  Lynch JP (2013) Steep, cheap and deep: an ideotype to optimize water and N acquisition by maize root systems.
412      Ann Bot 112:347–357. doi: 10.1093/aob/mcs293

413   Malamy JE (2005) Intrinsic and environmental response pathways that regulate root system architecture. Plant,
414         Cell Environ 28:67–77.

415   Mathieu L, Lobet G, Tocquin P, Périlleux C (2015) "Rhizoponics": a novel hydroponic rhizotron for root system
416         analyses on mature *Arabidopsis thaliana* plants. Plant Methods 11:1-7. doi: 10.1186/s13007-015-0046-x

417   Meister R, Rajani MS, Ruzicka D, Schachtman DP (2014) Challenges of modifying root traits in crops for
418         agriculture. Trends Plant Sci 19:779–788. doi: 10.1016/j.tplants.2014.08.005

419   Nagel KA, Putz A, Gilmer F, et al. (2012) GROWSCREEN-Rhizo is a novel phenotyping robot enabling
420         simultaneous measurements of root and shoot growth for plants grown in soil-filled rhizotrons. Funct Plant
421         Biol 39:891–904.

422   Pace J, Lee N, Naik HS, et al. (2014) Analysis of maize (*Zea mays* L.) seedling roots with the high-throughput
423         image analysis tool ARIA (Automatic Root Image Analysis). PLoS One 9:e108255. doi:
424         10.1371/journal.pone.0108255

425   Pagès L (2014) Branching patterns of root systems: quantitative analysis of the diversity among dicotyledonous
426         species. Ann Bot 114:591–598. doi: 10.1093/aob/mcu145

427   Pagès L, Bécel C, Boukcim H, et al. (2013) Calibration and evaluation of ArchiSimple, a simple model of root
428         system architecture. Ecol Modell 290:76–84. doi: 10.1016/j.ecolmodel.2013.11.014

429   Pound MP, French AP, Atkinson JA, et al. (2013) RootNav: navigating images of complex root architectures.
430         Plant Physiol 162:1802–1814. doi: 10.1104/pp.113.221531

431   R Core Team (2015) R: A language and environment for statistical computing. R Foundation for Statistical
432         Computing, Vienna, Austria. URL http://www.r-project.org/.

433   Rascher U, Blossfeld S, Fiorani F, et al. (2011) Non-invasive approaches for phenotyping of enhanced performance
434         traits in bean. Funct Plant Biol 38:968–983. doi: 10.1071/FP11164

435   Rich SM, Watt M (2013) Soil conditions and cereal root system architecture: review and considerations for linking
436         Darwin and Weaver. J Exp Bot 64:1193–1208. doi: 10.1093/jxb/ert043

437   Schmid C, Bauer S, Bartelheimer M (2015) Should I stay or should I go? Roots segregate in response to
438         competition intensity. Plant Soil 391:283–291. doi: 10.1007/s11104-015-2419-3

439   Slovak R, Göschl C, Su X, et al. (2014) A scalable open-source pipeline for large-scale root phenotyping of
440         *Arabidopsis*. Plant Cell 26:2390–2403. doi: 10.1105/tpc.114.124032

441   Thaler P, Pagès L (1996a) Root apical diameter and root elongation rate of rubber seedlings (*Hevea brasiliensis*)
442         show parallel responses to photoassimilate availability. Physiol Plant 97:365–371.

443   Thaler P, Pagès L (1996b) Periodicity in the development of the root system of young rubber trees (*Hevea
444         brasiliensis* Muell. Arg.): relationship with shoot development. Plant Cell Environ 19:56–64.

445   Uga Y, Sugimoto K, Ogawa S, et al. (2013) Control of root system architecture by *DEEPER ROOTING 1* increases
446         rice yield under drought conditions. Nat Genet 45:1097–1102. doi: 10.1038/ng.2725

447   Wells DM, French AP, Naeem A, et al. (2012) Recovering the dynamics of root growth and development using
448         novel image acquisition and analysis methods. Philos Trans R Soc B 367:1517–1524. doi:
449         10.1098/rstb.2011.0291

450   Wu J, Pagès L, Wu Q, et al. (2014) Three-dimensional architecture of axile roots of field-grown maize. Plant Soil
451         387:363–377. doi: 10.1007/s11104-014-2307-2

452    Zhu J, Ingram PA, Benfey PN, Elich T (2011) From lab to field, new approaches to phenotyping root system
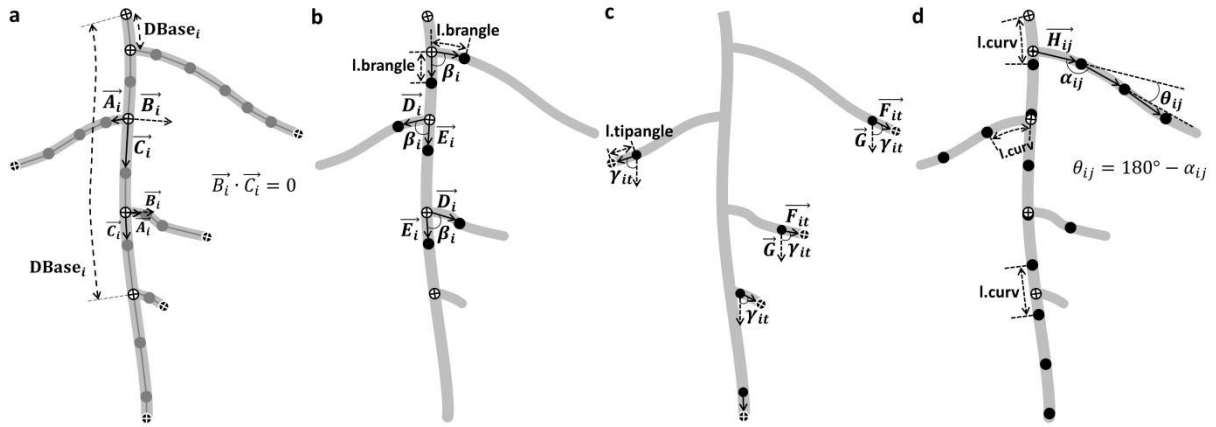453        architecture. Curr Opin Plant Biol 14:310–317. doi: 10.1016/j.pbi.2011.03.020

454

**Fig. 1 Computation of branching angles (b), root tip angles (c) and root curvatures (d) by *trajectory*.** (a) A simple root system after vectorization with a root image analysis software package. In Fig. 1a, the distance between the branching point and the parent root base (referred to as DBase in the text) is shown for two lateral roots. $\beta_i$, the branching angle of the root $i$ on its corresponding mother root; $\gamma_{it}$, the tip angle of the root $i$ at the observation date $t$; $\alpha_{ij}$, the angle $j$ between two successive links of the root $i$; $\theta_{ij}$, the angle $j$ between the direction vectors of two successive links of the root $i$. White dots with a black cross: branching points; black dots with a white cross: root tips; grey dots: points placed on the root system during the tracing of roots; black dots: new points linearly interpolated by *trajectory*
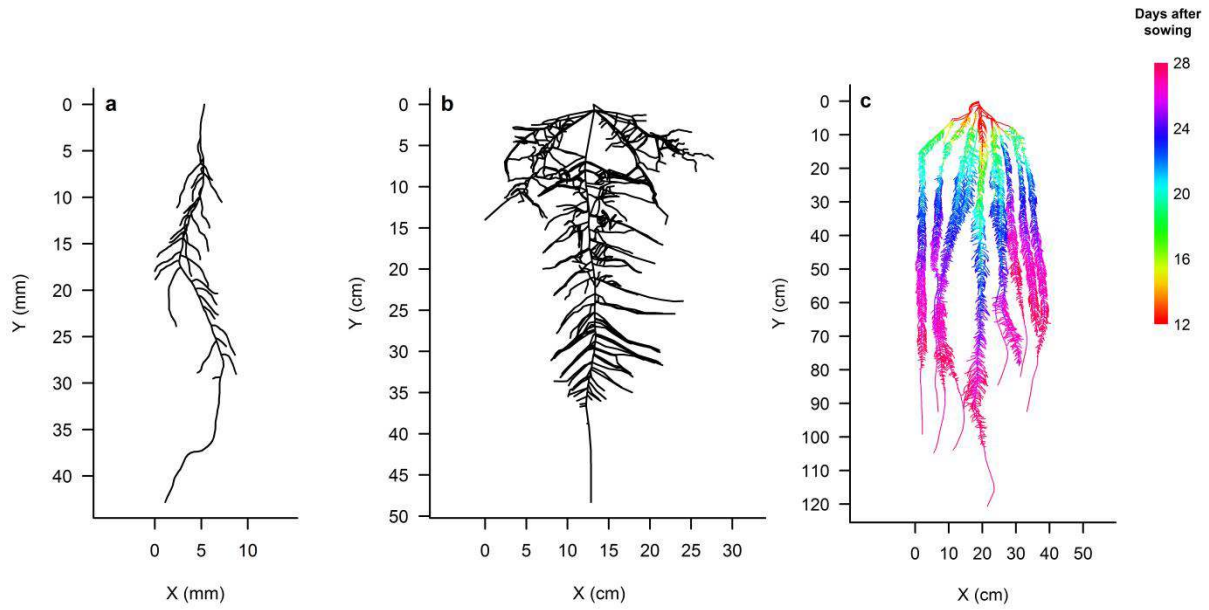
465

**Fig. 2 X-Y plotting of vectorized root systems using *archidraw*.** (a) A *B. distachyon* root system produced *in vitro* that was exposed for 11 days to volatiles emitted by *B. subtilis* AP305-GB03, (b) the root system of a 37-day-old *H. brasiliensis* seedling produced in a vertical rhizotron, and (c) part of the root system of a 28-day-old *S. lycopersicum* seedling produced hydroponically in a horizontal flat box. Each root system was plotted at the last observation date. The *S. lycopersicum* root system is shown with a specific colour for each observation date

471

472
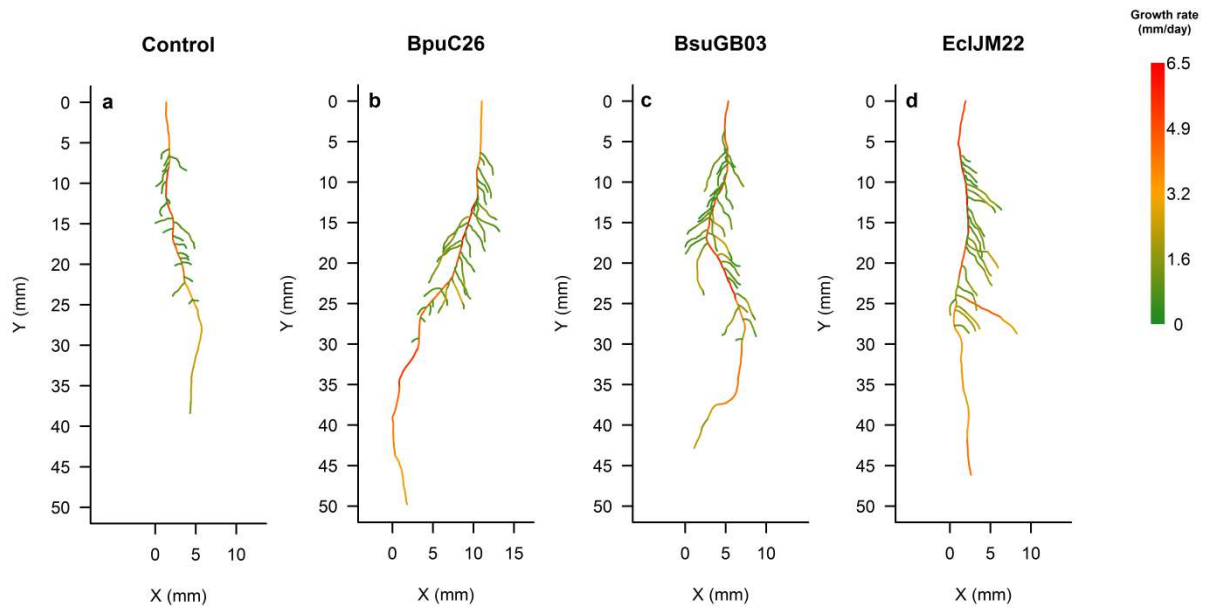
**Fig. 3 X-Y plotting of vectorized *B. distachyon* root systems using *archigrow*.** Plants were either cultivated

without PGPR (control) or exposed to volatiles emitted by *B. pumilus* C26 (BpuC26), *B. subtilis* AP305-GB03

(BsuGB03) or *E. cloaceae* AP12-JM22 (EclJM22) for 11 days. Each root system was plotted at the last observation

date. The colour code used for each link depends on its corresponding growth rate value and is shown at the right
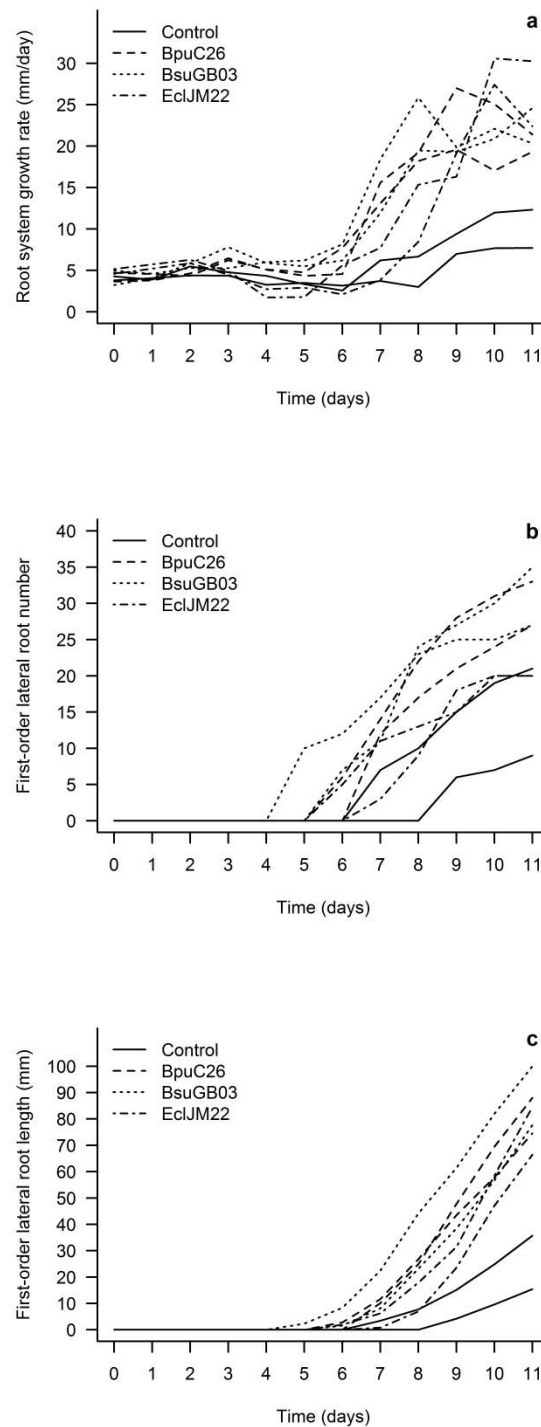
side of the plot

478

479

480 **Fig. 4 Evolution of the root system growth rate (a), the first-order lateral root number (b), and the first-**

481 **order lateral root length (c) of representative *B. distachyon* plantlets co-cultivated or not with PGPR**. Plants

482 were either cultivated without PGPR (control) or exposed to volatiles emitted by *B. pumilus* C26 (BpuC26), *B.*

483 *subtilis* AP305-GB03 (BsuGB03) or *E. cloaceae* AP12-JM22 (EclJM22) for 11 days. RSA parameters were
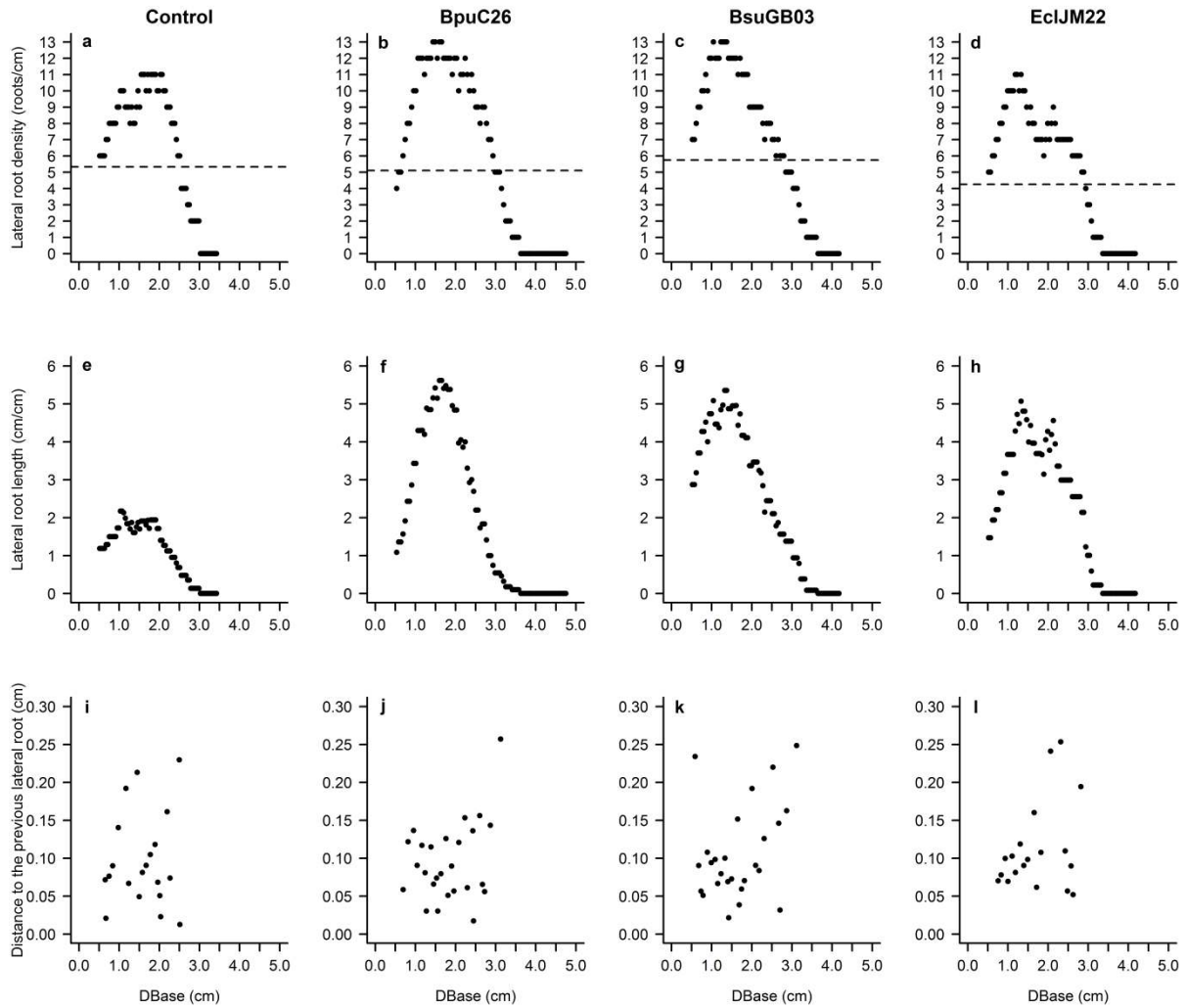
484 calculated using the function *architect*

**485**

**486** **Fig. 5 Analysis of the first-order lateral root density distribution (a-d), the first-order lateral root length**

**487** **distribution (e-h) and the inter-branch distance between neighbouring first-order lateral roots (i-l) on the**

**488** **primary root of representative *B. distachyon* plantlets co-cultivated or not with PGPR.** Plants were either

**489** cultivated without PGPR (control) or exposed to volatiles emitted by *B. pumilus* C26 (BpuC26), *B. subtilis* AP305-

**490** GB03 (BsuGB03) or *E. cloaceae* AP12-JM22 (EclJM22) for 11 days. DBase refers to the distance between the

**491** branching point of a first-order lateral root to the parent root base. Each horizontal dashed line refers to the mean

**492** secondary root density calculated by *latdist* along each primary root (Control: 5.3 roots/cm; BpuC26: 5.1 roots/cm;

**493** BsuGB03: 5.7 roots/cm; EclJM22: 4.3 roots/cm). Calculations were performed using the function *latdist* with an

**494** interval length of 1 cm and an interpolation value of 100
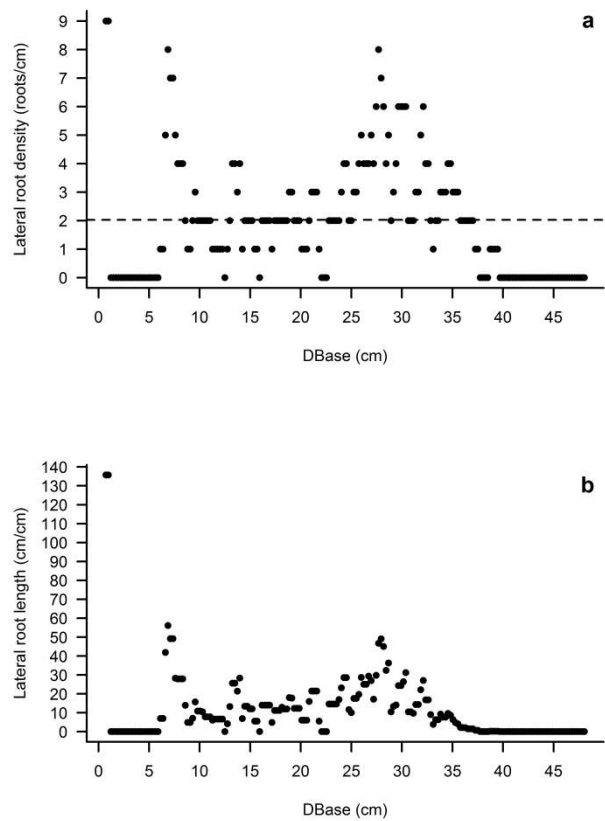
**495**

496

**Fig. 6 Analysis of the first-order lateral root density distribution (a) and the first-order lateral root length**

**distribution (b) along the taproot of a 37-day-old *H. brasiliensis* root system produced in a vertical rhizotron.**

DBase refers to the distance between the branching point of a first-order lateral root to the parent root base. The

horizontal dashed line refers to the mean secondary root density calculated by *latdist* along the taproot (2.0
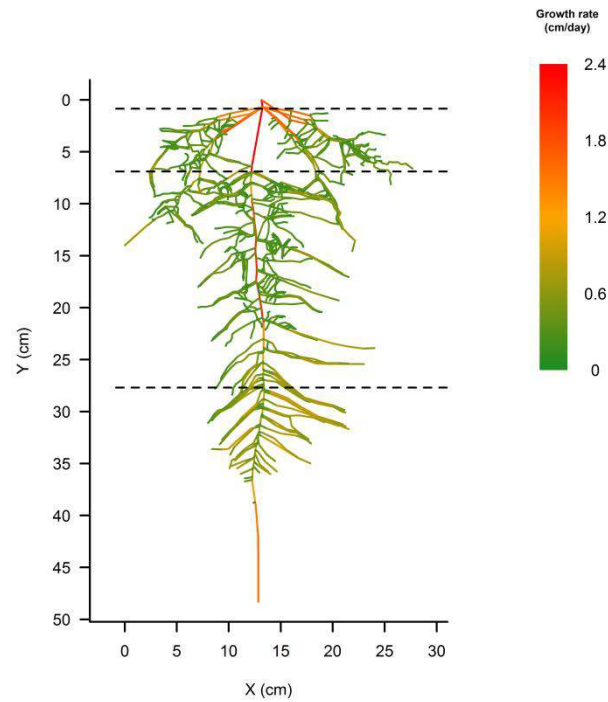
roots/cm)

502

503

**Fig. 7 X-Y plotting of a 37-day-old *H. brasiliensis* root system produced in a vertical rhizotron using**

*archigrow*. The root system was plotted at the last observation date. The colour code used for each link depends

on its corresponding growth rate value and is shown at the right side of the plot. Regions of the taproot associated

with high first-order lateral root densities are located at the intersection of the taproot and each horizontal dashed
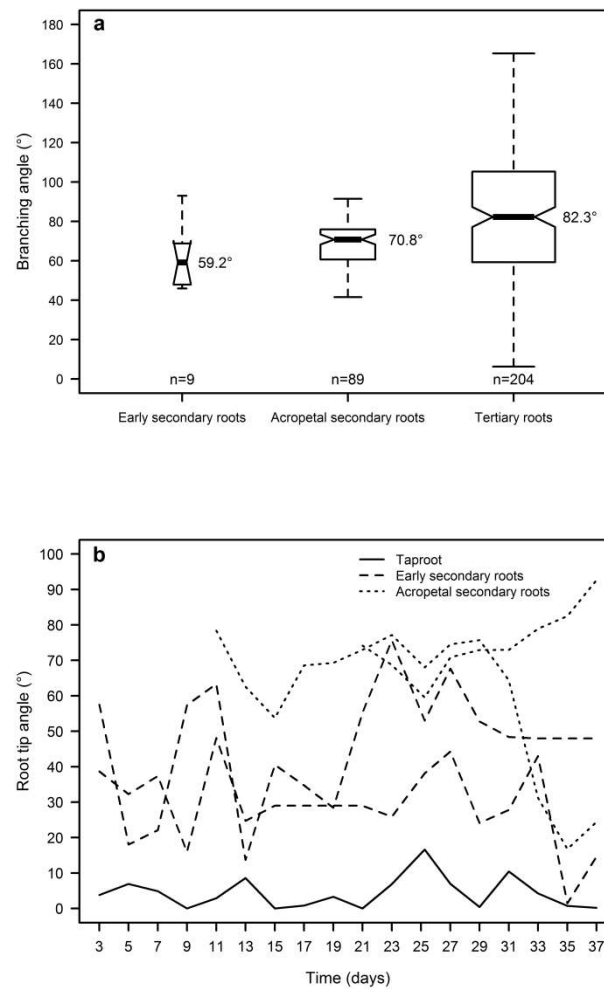
line

509

510

**Fig. 8 Analysis of the branching angles (a) and the gravitropism (b) of selected roots of a 37-day-old *H.***

**brasiliensis* root system produced in a vertical rhizotron.** In Figure a, the branching angles were calculated

separately for the main root types identified by Le Roux and Pagès (1994). In each boxplot, the whiskers were

extended to the most extreme data points localized between the hinges of the box and 1.5 times the interquartile

range. For clarity reasons, Figure b shows only the evolution of the root tip angle for the taproot, the two longest

early secondary roots and the two longest acropetal secondary roots. Calculations were performed using the

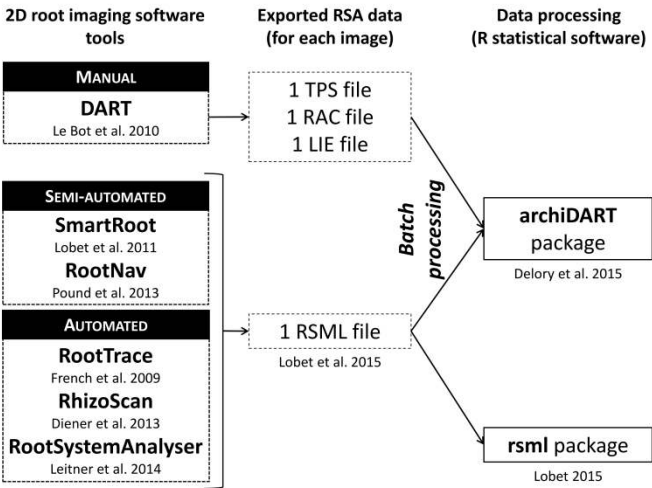*trajectory* function with the l.brangle and l.tipangle set at 0.5 cm

518

519

520 **Fig. 9 Root system architecture analysis pipeline: from data acquisition to data processing**

521 **Table 1 Overview of the required files, returned R objects and calculated RSA traits for each R function of**
522 **the archiDART package (version 1.1).** DART, Data Analysis of Root Tracings; RAC, DART-generated file
523 storing topological and length attributes for each individual root of a vectorized root system (file extension: .rac);
524 TPS, DART-generated file storing temporal attributes for each observation date (file extension: .tps); LIE, DART-
525 generated file storing spatial attributes for each point used to construct a vectorized root system (file extension:
526 .lie); RSML, Root System Markup Language; UT, the unit of time used by the experimenter; mm, millimetres;
527 cm, centimetres; px, pixels; d, degrees; r, radians

| R function | DART/RSML files | Returned R objects | RSA traits | Units |
|---|---|---|---|---|
| *archidraw* | LIE RSML | Plot window | × | × |
| *archigrow* | LIE + TPS | Plot window List | × Individual root growth rate at each observation date | × (mm, cm or px)/UT |
| *architect* | RAC + TPS RSML | Data frame | *For each observation date:* Length of the root system | mm, cm or px |
| | | | Growth rate of the root system | (mm, cm or px) /UT |
| | | | Length of the first-order root[a] | mm, cm or px |
| | | | Growth rate of the first-order root[a] | (mm, cm or px) /UT |
| | | | Total number of lateral roots | - |
| | | | Total length of lateral roots | mm, cm or px |
| | | | Total number of lateral roots by branching order | - |
| | | | Total length of lateral roots by branching order | mm, cm or px |
| | | | Mean length of lateral roots by branching order | mm, cm or px |
| | | | Growth rate of lateral roots by branching order | (mm, cm or px) /UT |
| | | | Density of secondary roots on the first-order root[a] | $mm^{-1}$, $cm^{-1}$ or $px^{-1}$ |
| | | | Secondary root number distribution on the first-order root[a] | - |
| | | | Secondary root length distribution on the first-order root[a] | mm, cm or px |
| | | | Secondary root density distribution on the first-order root[a] | $mm^{-1}$, $cm^{-1}$ or $px^{-1}$ |
| *latdist* | RAC RSML | List | *For each mother root:* Total number of lateral roots | - |
| | | | Mean lateral root density | $mm^{-1}$, $cm^{-1}$ or $px^{-1}$ |
| | | | Lateral root density distribution | $mm^{-1}$, $cm^{-1}$ or $px^{-1}$ |
| | | | Lateral root length distribution | mm/mm, cm/cm or px/px |
| | | | Distance to the previous lateral root (inter-branch distance) | mm, cm or px |
| *trajectory* | RAC + LIE + TPS RSML | List | Tortuosity | - |
| | | | Orientation | - |
| | | | Branching angle of each daughter root on its corresponding mother root | d or r |
| | | | The mean and the standard deviation of the local angle values calculated between the direction vectors of the successive links constructed using equidistantly spaced interpolated points along each root of a vectorized root system | d or r |
| | | | *For each observation date:* Root tip angle relative to a vertical direction vector | d or r |

528 [a] When analysing the topology of a root system, a first-order root is defined as a root that is directly connected to

529 the shoot.

530  **Table 2 Description of the RSA traits computed by the functions of the R package archiDART (version**
531  **1.1)**

| RSA traits | Description |
|---|---|
| Root length | The length of a root is calculated as the length of the polyline (i.e. a succession of linear segments) constituting the skeletonized root. Root length calculations are performed using the spatial and topological information exported from DART or using the geometry elements (SCENE > PLANT > ROOT > Geometry > polyline) stored in each RSML file. |
| Root number | The number of root elements constituting a skeletonized root system. |
| Root growth rate | For the first observation date, it is calculated as the ratio of the root length to the root system age. For other observation dates (t), it is calculated as the difference between the root length at time t and t-1 divided by the difference between the root system age at time t and t-1. |
| Lateral root density | For each mother root, it is calculated as the total number of daughter roots directly connected to the parent root divided by the length of the mother root. When evaluating the lateral root density distribution, the *latdist* function calculates local lateral root densities at intervals of a length defined by the experimenter and centred on points located at various distances from the parent root base. |
| Inter-branch distance | The distance separating a lateral root from its closest neighbour located at the greatest distance from the apex of the mother root. |
| Tortuosity | The ratio of the root length to the Euclidean distance between the root base and the apex. |
| Orientation (Fig. 1a) | Does a daughter root emerge at the left $(\overrightarrow{A_i} \cdot \overrightarrow{B_i} > 0)$ or the right $(\overrightarrow{A_i} \cdot \overrightarrow{B_i} < 0)$ side of the parent root? <br><br> $\overrightarrow{A_i}$ is a direction vector going from the branching point to the following point on the daughter root *i*. <br><br> $\overrightarrow{B_i}$ is a vector orthogonal to a direction vector going the branching point to the following point on the mother root of the root *i*. In this paper, we consider that the normal vector that is orthogonal to a direction vector (a,b) will have the following coordinates: (b,-a). |
| Branching angle (Fig. 1b) | The branching angle $\beta_i$ of the root *i* on its parent root is calculated according to the following equation: $$\beta_i = \cos^{-1}\left(\frac{|\overrightarrow{D_i}\cdot\overrightarrow{E_i}|}{\|\overrightarrow{D_i}\|\cdot\|\overrightarrow{E_i}\|}\right)$$ $\overrightarrow{D_i}$ is a direction vector going from the branching point to a linearly interpolated point located at a user-specified distance (l.brangle) from the branching point on the daughter root *i*. <br><br> $\overrightarrow{E_i}$ is a direction vector going from the branching point to a linearly interpolated point located at a user-specified distance (l.brangle) from the branching point on the parent root of the root *i*. |
| Root tip angle (Fig. 1c) | The tip angle $\gamma_{it}$ of the root *i* at the observation date *t* is calculated according to the following equation: $$\gamma_{it} = \cos^{-1}\left(\frac{|\overrightarrow{F_{it}} \cdot \vec{G}|}{\|\overrightarrow{F_{it}}\| \cdot \|\vec{G}\|}\right)$$ $\overrightarrow{F_{it}}$ is a direction vector going from a linearly interpolated point placed along the root *i* at a user-defined distance from the apex (l.tipangle) to the root tip. <br><br> $\vec{G}$ is a vertical direction vector. |
| Root curvature (Fig. 1d) | The curvature of the root *i* is evaluated by statistical parameters (mean and standard deviation) describing the distribution of local angles $(\theta_{ij})$ measured along each root following the method proposed by French et al. (2009). |

532

27